Electronic structure of the weakly coupled edge-sharing MnO_4 spin-$\frac{5}{2}$ chain compound $LiMnVO_4$: an *ab initio* study

2008 J. Phys.: Condens. Matter 20 395204

(http://iopscience.iop.org/0953-8984/20/39/395204)

IOP PUBLISHING JOURNAL OF PHYSICS: CONDENSED MATTER

J. Phys.: Condens. Matter **20** (2008) 395204 (9pp) doi:10.1088/0953-8984/20/39/395204

Electronic structure of the weakly coupled edge-sharing MnO_4 spin-$\frac{5}{2}$ chain compound $LiMnVO_4$: an *ab initio* study

Xing Ming[1], Chun-Zhong Wang[1], Hou-Gang Fan[1,2], Fang Hu[1], Ying-Jin Wei[1], Zu-Fei Huang[1,3], Xing Meng[1] and Gang Chen[1,4]

[1] Department of Materials Science, College of Materials Science and Engineering, Jilin University, Changchun 130012, People's Republic of China
[2] College of Physics, Jilin Normal University, Siping 136000, People's Republic of China
[3] College of Physics, Jilin University, Changchun 130012, People's Republic of China

E-mail: gchen@jlu.edu.cn

Received 23 April 2008, in final form 7 August 2008
Published 1 September 2008
Online at stacks.iop.org/JPhysCM/20/395204

Abstract

Based on fully self-consistent first-principles density functional theory (DFT) calculations as well as classical spin analysis, we study the electronic structure and magnetic interactions of the spinel-related compound $LiMnVO_4$. Four possible ordered spin states have been considered by spin-polarized generalized gradient approximation (GGA) calculations. The antiferromagnetic (AFM) configuration with both intra-chain and inter-chain AFM coupling interactions is energetically favorable among these magnetic ordered states. The calculated AFM solution agrees well with a series of experimental measurements. The intra-atomic exchange splitting of the Mn 3d spin-up and spin-down states results in the insulating behavior of $LiMnVO_4$. The Heisenberg Hamiltonian is used to deduce the magnetic coupling parameters by adopting Noodleman's broken symmetry method. The intra-chain AFM interactions are much stronger than the inter-chain AFM interactions and thus $LiMnVO_4$ can be described as a weakly coupled edge-sharing spin $\frac{5}{2}$ chain system. We propose that the presence of the side groups of edge-sharing LiO_4 and VO_4 tetrahedra are contributing to the intra-chain AFM interactions in the nearly 90° Mn–O–Mn bond configuration of the edge-sharing MnO_4 chains.

(Some figures in this article are in colour only in the electronic version)

1. Introduction

The transition-metal oxides (TMOs) have been a group of materials in the focus of condensed matter physics. As a result of the interplay between lattice, charge, spin and orbital degrees of freedom, TMOs exhibit fascinating phenomena and exotic properties. These phenomena and properties include metal–insulator transition (MIT), high-temperature superconductivity, colossal magnetoresistance (CMR), charge ordering, orbital ordering and electronic phase separation [1]. The intriguing phenomena and properties have attracted much attention and have been investigated extensively.

The compounds that are formed with the well known cubic spinel structure are a class of important TMOs and have been studied intensively [2]. The spinel compounds are expressed by the chemical formula AB_2O_4, where oxygen ions are localized in a face-centered-cubic (fcc) close-packed lattice. Spinel structure can be classified into normal and inverse spinels. In normal spinel structure compounds, A ions reside in the tetrahedral sites and B ions occupy the octahedral sites. In the case of inverse spinel compounds, A ions and half of the B ions are located on the octahedral sites; the other half of the B ions occupy the tetrahedral sites. Due to the three-dimensional geometrical frustration, complicated electronic and magnetic properties emerge when the octahedral sites are occupied by the magnetic transition-metal (TM) ions in a normal spinel compound [2, 3].

Among a wide variety of the normal spinel TMOs, the charge neutrality requires B ions to be in a mixed-valence

[4] Author to whom any correspondence should be addressed.

state, while the A ions are monovalent. For instance, lithium–manganese oxide ($LiMn_2O_4$) has a cubic spinel structure at room temperature, which has been widely investigated as a cathode material for rechargeable Li ion batteries [4], where equal numbers of Mn^{3+} and Mn^{4+} ions randomly distribute over the octahedral sites. The complicated structural transition and magnetic state of $LiMn_2O_4$ have been under extensive study [5–7]. Another typical compound with the normal spinel structure is lithium–vanadium oxide (LiV_2O_4), which has attracted great interest since its heavy-Fermi-liquid behavior was discovered by Kondo *et al* [8]. LiV_2O_4 is the first d-electron TMO system that shows heavy-fermion characteristics, whereas the conventional heavy-fermion compounds are f-electron compounds [8]. The origin of this heavy-fermion behavior in LiV_2O_4 is still under intensive dispute [9–11].

Stimulated by the exotic characteristics of $LiMn_2O_4$ and LiV_2O_4, we direct our attention to lithium–manganese vanadate $LiMnVO_4$—a compound in the pseudo-binary system of $LiMn_2O_4$ and LiV_2O_4 [12]. The crystal structure was identified by Rietveld analysis with an orthorhombic spinel-related structure (space group $Cmcm$, $Z = 4$) [12]. Powder neutron diffraction [13] confirmed this special structure. In $LiMnVO_4$, the edge-sharing MnO_6 octahedra form infinite MnO_4 chains with nearly 90° Mn–O–Mn bond angles. The edge-sharing MnO_4 chains are running parallel to the crystallographic c axis. As shown in figure 1, the MnO_6 octahedra are connected by pairs of edge-sharing LiO_4 and VO_4 tetrahedra. Padhi *et al* [14] reported that $LiMnVO_4$ transformed from the ambient-pressure orthorhombic phase to a high-pressure cubic spinel phase under a pressure of 55 kbar at 850 °C. Recently, a detailed single-crystal structure analysis to confirm the structure of $LiMnVO_4$ has been reported by Sugahara *et al* [15].

Although the crystal structure of $LiMnVO_4$ has been determined unambiguously, there are only a few experimental investigations on its properties and characteristics. Based on the magnetic susceptibility and the metal–oxygen bond distances estimated from the refined structure of $LiMnVO_4$, the valence states for the TM ions are assigned to divalent for Mn ions and pentavalent for V ions [13]. Furthermore, electron energy loss spectra (EELS) are also employed to investigate the electronic states of $LiMnVO_4$ [16]. The Mn L multiplet structure revealed that the electron configuration of Mn ions at octahedral sites is $3d^5$ (Mn^{2+}). The V L spectrum showed a characteristic multiplet structure in tetrahedral coordination d^0 (V^{5+}) compounds. The O K spectra revealed that the lowest unoccupied states of $LiMnVO_4$ are mainly V 3d bands and that the V–O bonding is partial covalent. Magnetic susceptibility measurements indicate that the chains of edge-sharing MnO_6 octahedra are antiferromagnetic (AFM) coupled along the c axis [14]. The electrical conductivity measurement indicated that $LiMnVO_4$ is insulating; an activation energy of 0.6 eV was extracted from the Arrhenius plots [17].

Recently, the quasi-one-dimensional (1D) Cu^{2+} ($3d^9$, $S = 1/2$) spin system, especially the edge-sharing Cu–O chain compounds with nearly 90° Cu–O–Cu bonds, have attracted great interest because of their unique electronic states and

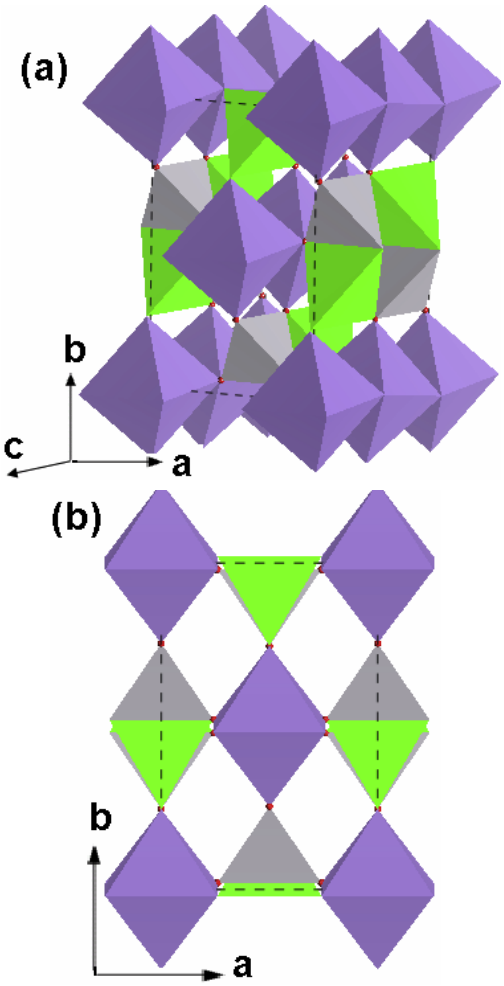

Figure 1. The crystal structural perspective polyhedral views of $LiMnVO_4$. The octahedra, gray tetrahedra and the fuscous tetrahedra represent the MnO_6 octahedra, the VO_4 tetrahedra and the LiO_4 tetrahedra.

magnetic properties, which are in striking contrast to the corner-sharing Cu–O chain with 180° Cu–O–Cu bonds [18]. According to the Goodenough–Kanamori–Anderson (GKA) rules [19], the nearest-neighbor (NN) Cu–Cu spin exchange interaction changes from AFM to ferromagnetic (FM) as the angle of the Cu–O–Cu bond is transformed from 180° to 90°. Due to the competition between FM and AFM exchange interactions, the quasi-1D edge-sharing Cu–O chain compounds display a variety of unusual phenomena. For example, the quasi-1D frustrated antiferromagnet $LiCuVO_4$ with edge-sharing CuO_4 units has been investigated intensively for its incommensurate noncollinear spiral-magnetic structure and ferroelectricity [20]. Park *et al* [21] discovered a ferroelectric (FE) polarization in the spiral-magnetic state of the 1D $S = 1/2$ cuprate $LiCu_2O_2$, which is the first example of an FE cuprate with an edge-sharing plate extending along the chain b direction and a ∼94° NN superexchange route along the b axis. Another typical cuprate is Li_2CuO_2 with edge-sharing CuO_2 chains, where three-dimensional (3D) AFM ordering occurs at $T_N = 8.3$ K arising from the anti-alignment of FM chains [22]. In addition, the side

group effects induce AFM coupling interactions in the edge-sharing CuO_2 square plane, which gives rise to the spin–Peierls transition in the first inorganic compound $CuGeO_3$ [23]. Inspired also by the structural comparability between edge-sharing MnO_4 chain and Cu–O chain compounds, we, for the first time, perform a systematic investigation of the electronic and magnetic properties for this edge-sharing MnO_4 chain compound $LiMnVO_4$ based on the *ab initio* electronic structure calculation.

The present work reports the detailed electronic structure of the orthorhombic-structural $LiMnVO_4$ by first-principles spin-polarized calculations based on the density functional theory (DFT). From the viewpoint of energy, the ground state of $LiMnVO_4$ is the AFM state with both intra-chain and inter-chain magnetic moments AFM aligned. The experimental insulating behavior has been successfully reproduced; the $3d^5$ configurations of the octahedral coordinated high-spin Mn^{2+} ions and tetrahedral coordinated V^{5+} ($3d^0$) ions have also been successfully simulated. The intra-atomic exchange splitting of the spin-up and spin-down Mn 3d states results in the insulating nature of $LiMnVO_4$. The spin exchange parameters are then obtained by mapping the relative energies of the four ordered spin states onto the Heisenberg spin Hamiltonian by employing the Noodleman's broken symmetry (BS) method [24–26]. The intra-chain AFM interactions are much stronger than the inter-chain AFM interactions. The side groups of pairs of edge-sharing LiO_4 and VO_4 tetrahedra contribute to the intra-chain AFM interaction in the nearly 90° Mn–O–Mn configuration of the edge-sharing MnO_4 chains. $LiMnVO_4$ is a weakly coupled edge-sharing MnO_4 AFM chain system.

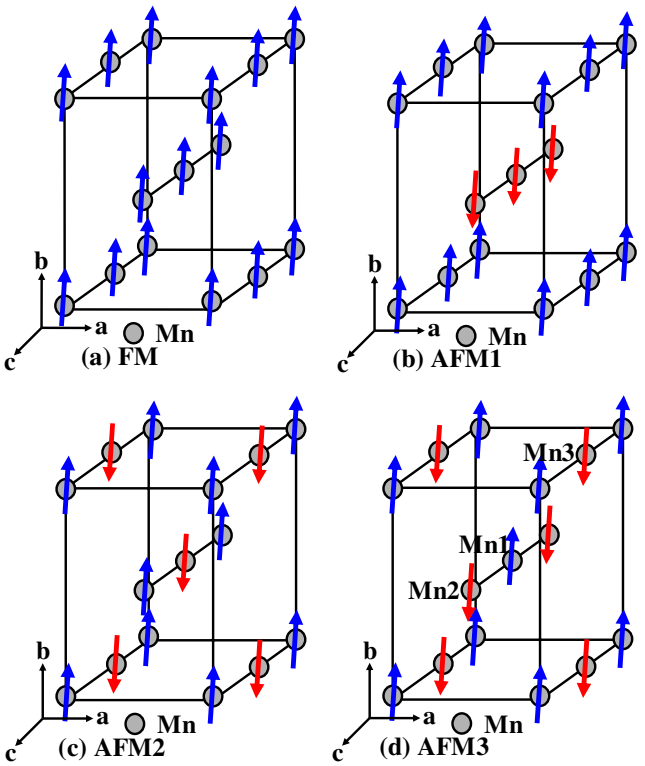

Figure 2. Schematic representations of the four hypothetical ordered spin arrangements in the $LiMnVO_4$ unit cell (only Mn ions are shown for clarity). The small gray spheres denote the Mn sites; the up (down) arrows represent the magnetic moment orientations.

2. Computational details

All-electronic structure calculations employ the DFT plane-wave pseudo-potential method as implemented in the CASTEP program [27]. The spin-polarized (spin-unrestricted) generalized gradient approximation (GGA) [28] is used to treat the exchange–correlation function within the PW91 form [29]. The interactions between the core region and valence electrons are described by a Vanderbilt-type ultrasoft pseudo-potential [30]. Li $1s^2\ 2s^1$, Mn $3d^5\ 4s^2$, V $3s^2\ 3p^6 3d^3\ 4s^2$ and O $2s^2\ 2p^4$ are treated as valence electrons during calculations. The cut-off energy of the plane-wave basis set is set to 380 eV for all calculations. The requested k-point spacing is set to 0.04 $Å^{-1}$, which corresponds to a k-point mesh of $4 \times 3 \times 4$ in the irreducible Brillouin zone generated by the special k-point sampling scheme of the Monkhorst–Pack method. Geometry optimizations are performed to fully relax the crystal structure model within the BFGS minimization algorithm [31]. The convergence thresholds for energy change, maximum force, maximum stress and maximum displacement between optimization cycles are 5×10^{-6} eV/atom, 0.01 eV $Å^{-1}$, 0.02 GPa and 5×10^{-4} Å.

The crystal structure model is built according to the experimental single-crystal structure data [15]. The crystal structure is first fully relaxed to optimize the atomic internal coordinates and the lattice parameters. The optimized structures are then used to carry out the calculations of total energy and the electronic structure. Since the formal valence state of the Mn ion is +2 with high-spin $3d^5$ configuration [13, 14, 16], we assign artificially four special ordered spin states (i.e., FM, AFM_1, AFM_2 and AFM_3) in the crystallographic unit cell.

As schematically shown in figure 2, the hypothetical FM state corresponds to an FM alignment of all magnetic moments, both intra-chain and inter-chain (figure 2(a)), whereas the other three AFM states are symmetry broken arrangements: FM chains are AFM coupled in the AFM_1 state (figure 2(b)); in the second AFM state (AFM_2), the intra-chain magnetic moments in each MnO_4 chain are AFM aligned, but the magnetic moments of adjacent MnO_4 chains are FM aligned (figure 2(c)); in the third AFM case (AFM_3), both intra-chain and inter-chain magnetic moments are AFM aligned (figure 2(d)). In consideration of the computational conditions, we just calculate the geometry of the FM state. The structural parameters of other three AFM ordered states are based on the FM one. The fully self-consistent spin-polarized DFT calculations are carried out to obtain the total energy and electronic structure based on these magnetic structures. Then the values of the nearest-neighbor magnetic exchange parameters are evaluated by mapping the relative energies of the four magnetic ordered states onto the Heisenberg spin Hamiltonian by employing the Noodleman's BS method [24–26].

Table 1. Calculated and experimental lattice parameters together with atomic internal coordinate parameters given in fractional coordinates (x, y, z). For the convenience of comparison, the position coordinates have been transformed according to the symmetry operators: (1) x, y, z; (2) $-x, -y, z + 1/2$; (3) $-x, y, -z + 1/2$; (4) $x, -y, -z$; (5) $-x, -y, -z$; (6) $x, y, z - 1/2$; (7) $x, -y, z + 1/2$; (8) $-x, y, z$; (9) $x + 1/2, y + 1/2, z$; (10) $-x + 1/2, -y + 1/2, z + 1/2$; (11) $-x + 1/2, y + 1/2, -z + 1/2$; (12) $x + 1/2, -y + 1/2, -z$; (13) $-x + 1/2, -y + 1/2, -z$; (14) $x + 1/2, y + 1/2, -z + 1/2$; (15) $x + 1/2, -y + 1/2, z + 1/2$; (16) $-x + 1/2, y + 1/2, z$.

	a (Å)	b (Å)	c (Å)	Atomic internal coordinates
This work	5.829	8.708	6.335	Li (0.500, 0.163, 0.250) Mn (0.000, 0.000, 0.000) V (0.000, 0.356, 0.250) O1 (0.238, 0.481, 0.250) O2 (0.000, 0.256, 0.029)
Experiment[a]	5.747	8.701	6.349	Li (0.500, 0.168, 0.250) Mn (0.000, 0.000, 0.000) V (0.000, 0.357, 0.250) O1 (0.236, 0.475, 0.250) O2 (0.000, 0.248, 0.037)
Experiment[b]	5.761	8.746	6.350	Li (0.500, 0.167, 0.250) Mn (0.000, 0.000, 0.000) V (0.000, 0.357, 0.250) O1 (0.237, 0.479, 0.250) O2 (0.000, 0.257, 0.035)
Experiment[c]	5.764	8.742	6.363	Li (0.500, 0.164, 0.250) Mn (0.000, 0.000, 0.000) V (0.000, 0.357, 0.250) O1 (0.241, 0.480, 0.250) O2 (0.000, 0.246, 0.032)

[a] Reference [12].
[b] Reference [14].
[c] Reference [15].

3. Results and discussion

3.1. Electronic structure

The calculated lattice parameters (a, b and c) and atomic internal coordinate parameters of $LiMnVO_4$ are listed together with the experimental data in table 1. Satisfactory agreement is reached between the DFT calculations and experimental results. The local spin magnetic moment (Li, Mn, V and O) and the total magnetic moment per unit cell for the four magnetic ordered states together with their relative energies are summarized in table 2. As shown in table 2, four ordered spin states and the high-spin $3d^5$ half-filled configuration of Mn^{2+} ions have been simulated successfully, which are in line with the experimental data [13, 14, 16]. According to the present spin-polarized calculations, the relative energies of the four ordered spin states decrease in the order FM > AFM_1 > AFM_2 > AFM_3. The AFM states are more stable with respect to the FM state from the viewpoint of energy, which is in good agreement with the susceptibility measurements [14]. Yahia *et al* [32] only took into account three ordered spin states for the isostructural compound $CuMnVO_4$; they neglected the AFM_1 state considered in the present work. Our calculated results are in agreement with [32]; the relative energies as well as the order of the four ordered spin states are very similar to the case of $CuMnVO_4$. The AFM state with both intra-chain and inter-chain AFM alignments of all magnetic moments is the lowest-energy state among all magnetic ordered states for $CuMnVO_4$ and $LiMnVO_4$. In contrast to $CuMnVO_4$, our calculated magnetic moments are closer to the ideal expected value of 5 for the high-spin $3d^5$ configuration of Mn^{2+} ions. The detailed magnetic coupling interactions will be discussed in section 3.2.

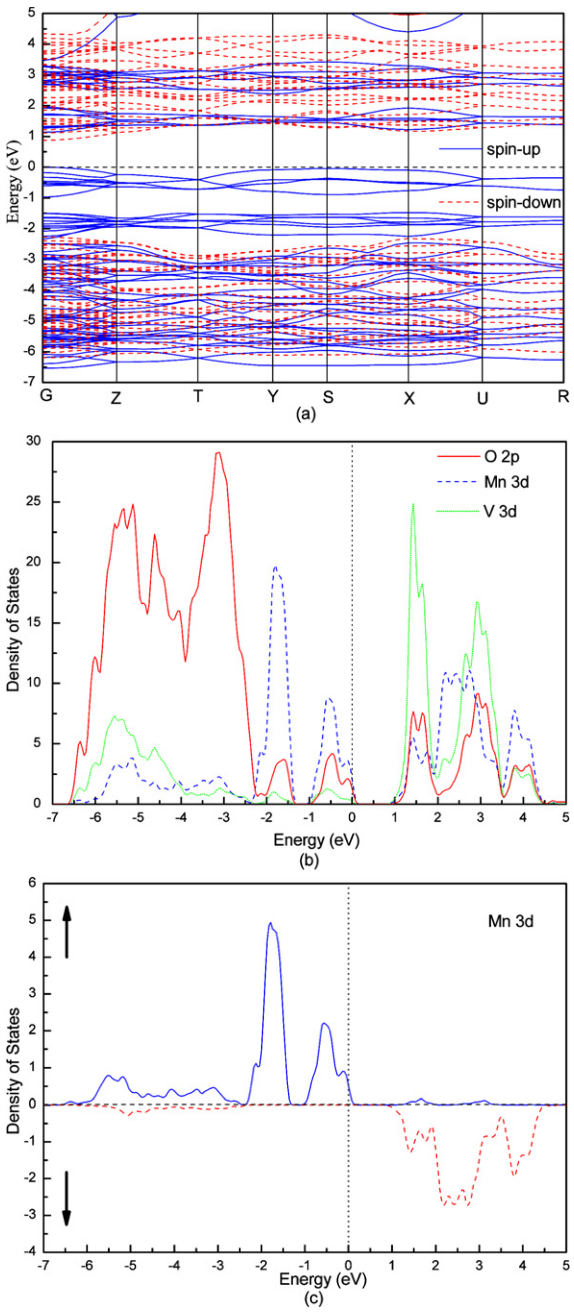

Figure 3. Electronic structure of ferromagnetic (FM) state $LiMnVO_4$. (a) The band structure. (b) The corresponding atom-resolved partial density of states (PDOS) for O 2p states (solid line), Mn 3d states (dashed line) and V 3d states (dotted line). (c) Spin-projected PDOS for Mn 3d states; spin-up/down states are plotted along the positive/negative ordinate.

Figure 3 shows the energy band structure and corresponding partial density of states (PDOS) for the FM state, where

Table 2. Calculated values of the local spin magnetic moment (Li, Mn, V and O), the total magnetic moment, the relative energies per formula unit and the band gap value of the four spin configurations.

	Local spin magnetic moment (μ_B)							
	M_{Li}	M_{Mn}	M_V	M_{O1}	M_{O2}	M_{Tot}	Relative energy (meV)	Band gap (eV)
FM	0	4.62	0.30	0	0	5	0	0.90
AFM_1	0	±4.62	0	0	0	0	−7.6	1.15
AFM_2	0	±4.64	0	0	0	0	−26.5	1.22
AFM_3	0	±4.64	0	0	0	0	−33.3	1.45

the zero of energy is set as the Fermi level (E_F). In the band structure (figure 3(a)), the spin-up/down subbands are plotted with solid/dashed lines respectively. The lower parts of the valence bands are formed primarily from O 2p orbitals hybridized with partial V 3d orbitals, which are almost separated from the upper 20 spin-up valence bands below E_F. The isolated 20 spin-up valence bands are almost all derived from the 3d orbitals of the four Mn atoms in the unit cell, which is consistent with $3d^5$ configuration of the high-spin Mn^{2+} ions [13, 14, 16]. The Mn 3d valence bands are split further by the MnO_6 octahedral crystal field into the eight upper e_g bands and 12 lower t_{2g} bands [16]. The conduction bands above E_F are separated by an insulating energy gap of about 0.90 eV from the top of the valence bands, which are derived mainly from V 3d orbitals and Mn 3d orbitals (spin down) with partial O 2p antibonding hybridization orbitals. From the spin projected PDOS of Mn 3d states shown in figure 3(c), we can see that the Mn 3d spin-up orbitals are fully occupied, whereas the spin-down orbitals are fully empty, which are very close to the spin projected PDOS of the Mn half-filled 3d bands in $CuMnVO_4$ [32]. This characteristic reveals the $3d^5$ configuration of the high-spin Mn^{2+} ions, which is consistent with the divalent manganese revealed by a series of experiments [13, 16]. Moreover, Mn 3d electrons are entirely spin polarized; the intra-atomic exchange splitting results in the insulating behavior of $LiMnVO_4$ [17]. The primary characteristics of electronic structure for the FM state are almost the same as those of $CuMnVO_4$. In $CuMnVO_4$, the half-filled 3d bands of Mn^{2+} lie lower than the completely filled 3d bands of Cu^+, and the separation between O 2p bands and Mn^{2+}/Cu^+ 3d bands is more distinct [32].

The electronic band structures of the three symmetry broken AFM states (as shown in figures 2(b)–(d)) are displayed in figure 4. One remarkable characteristic of the energy bands for these AFM states are that the spin-up and spin-down subbands overlap each other. These two spin states are absolutely identical at the same energy, exhibiting the unique characteristic of the AFM ordering. The essential characteristics of the band structure of these AFM states are almost the same. The lower parts of the valence bands are derived mainly from O 2p orbitals. Different from the FM state, the O 2p bands are separated distinctly from the Mn 3d valence bands by a gap in these AFM states. In addition, the Mn 3d valence bands in AFM states are much narrower and the crystal-field splittings between the e_g bands and t_{2g} bands are enlarged relative to the FM state. As shown in figure 4, the differences among these AFM states are, along with the energy decreasing (refer to table 2), that the width of the e_g bands and t_{2g} bands of the Mn 3d valence bands decreases gradually and the insulating gap becomes larger and larger. Compared with the AFM_2 state of $CuMnVO_4$, the width of the e_g bands and t_{2g} bands of the Mn 3d valence bands is narrower and the crystal-field splitting between them is larger in $LiMnVO_4$ [32]. These narrow band characteristics of the Mn 3d valence bands reflect the localized nature of the Mn $3d^5$ electrons in these AFM spin-ordered states.

As already mentioned, the AFM_3 state is energetically favorable among all four magnetic ordered states, and therefore the ground state of $LiMnVO_4$–AFM_3 is characterized with both nearest-neighbor intra-chain and inter-chain magnetic moment all antiparallel aligned. The electronic structure of the AFM_3 state is going to be mainly discussed.

The total DOS and atom-resolved PDOS have been displayed in figure 5(a). The formal valence state of V ions is pentavalent with $3d^0$ configuration. Nevertheless, the valence bands have shown some V 3d state character presented in figure 5(a). This characteristic reflects the partial covalence of the tetrahedral coordinated V ions with O ions as shown in EELS [16]. In order to inspect the occupied states of Mn 3d electrons, we select Mn ions on three different sites: the Mn ion in the center of the unit cell, adjacent intra-chain Mn ions along the infinite MnO_4 chain and the nearest-neighbor inter-chain Mn ions perpendicular to the chain (as shown in figure 2(d), marked as Mn1, Mn2 and Mn3). Figure 5(b) shows the corresponding site-resolved spin-projected PDOS for these three kinds of Mn ions. It is obvious that Mn^{2+} ions are in high-spin $3d^5$ configuration; the nearest-neighbor spin moments are antiparallel (AFM coupled) to each other both along the same chains and between the nearest-neighbor chains. These prominent characters of the AFM_3 magnetic ordering are nearly the same as the case of the AFM_2 state in $CuMnVO_4$, as shown in figure 8 in [32]. It should be noted that, due to the Gaussian smearing, there are tails at the Fermi level, but the insulating nature has been reproduced successfully, as proved by the band structure shown in figures 3(a) and 4.

To further examine the detailed features of the electronic states in this complicated AFM compound $LiMnVO_4$, it is useful to plot the electronic-spin density of the valence bands for its ground state spin configuration. We direct our attention mainly to three distinct energy ranges extending from −6.1 eV to the Fermi level, as shown in figure 6. As seen in the PDOS plots of figure 5(a), the lower valence bands for energy range I (−6.1 to −2.2 eV) correspond to primary O 2p states, in the energy ranges II (−1.7 to −1.2 eV) and III (−0.4 to 0 eV) are primary Mn 3d states. In the AFM ground state, Mn 3d

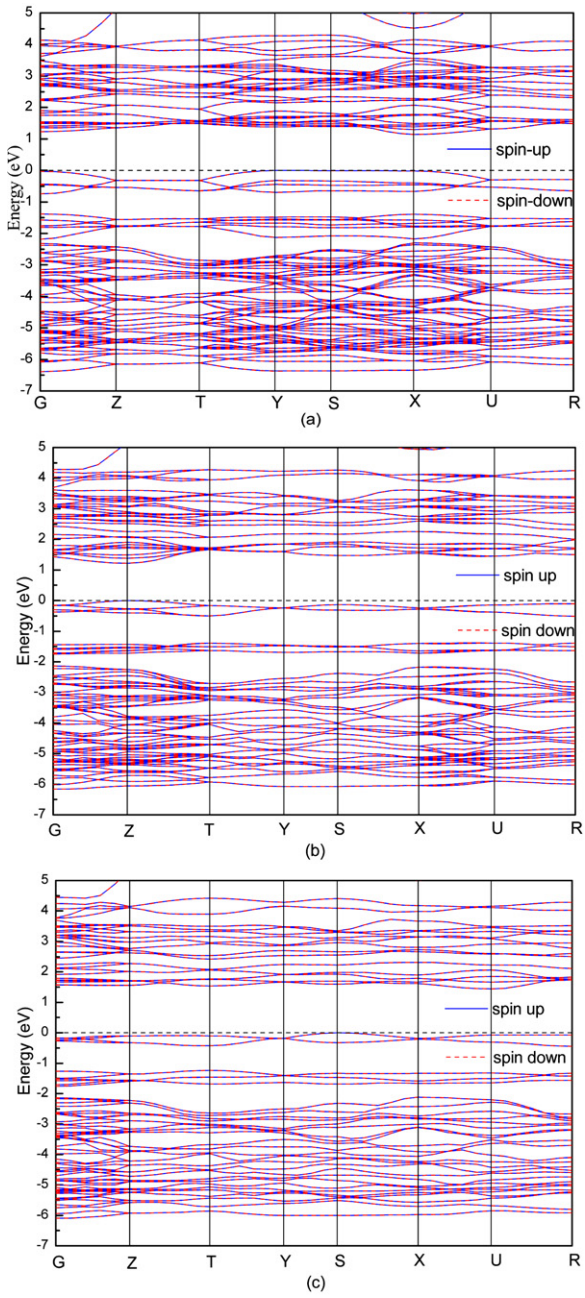

Figure 4. Electronic band structure of $LiMnVO_4$ for the three antiferromagnetic (AFM) states: (a) AFM_1 state, (b) AFM_2 state and (c) AFM_3 state. Spin-up/down subbands are plotted with solid/dashed lines. Because of the AFM ordering, the spin-up/down subbands overlap each other.

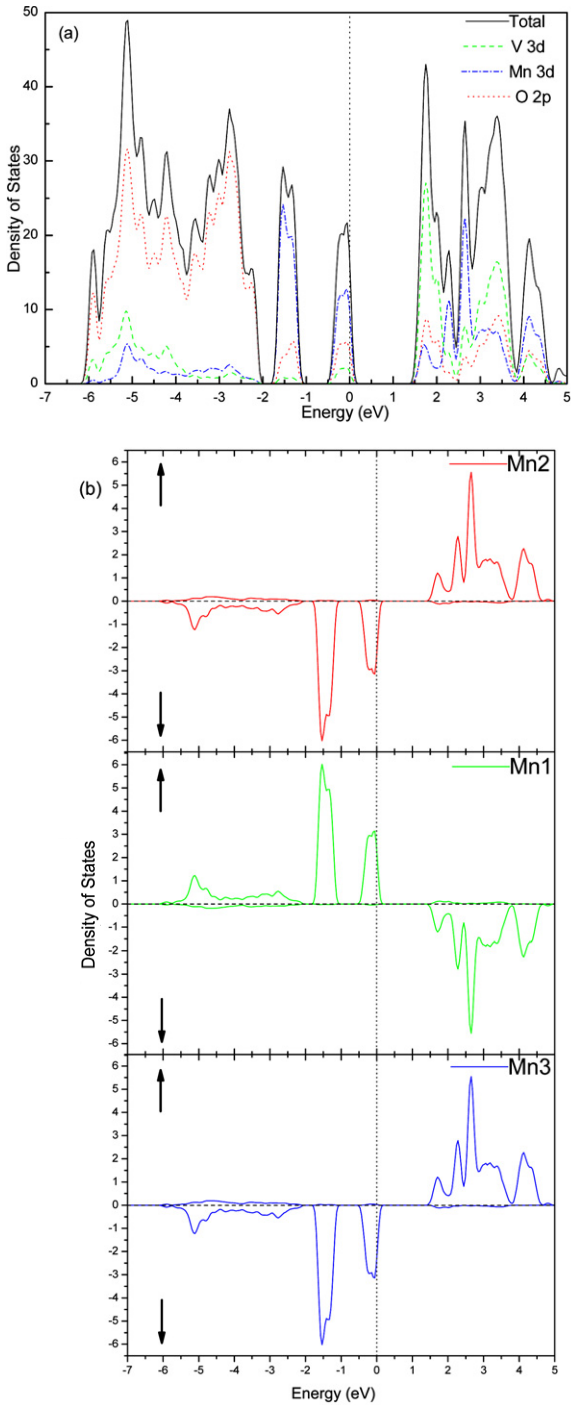

Figure 5. Density of states (DOS) and corresponding partial DOS (PDOS) for the AFM_3 state of $LiMnVO_4$: (a) the total DOS and corresponding atom-resolved PDOS; (b) the site-resolved spin projected PDOS for Mn ions on three sites as shown in figure 2(d). Spin-up/down states are plotted along the positive/negative ordinate.

electrons are fully spin polarized; the spins are antiparallel to each other both along and between adjacent MnO_4 chains. The orbital orientations of the electronic-spin densities in regions II and III of figure 6 show visually the t_{2g} and e_g states on the Mn sites, respectively. It is apparent that the Mn 3d valence bands are split into separated lower-energy t_{2g} bands (figure 6(b)) and higher-energy e_g bands (figure 6(c)), which agrees well with the local crystal symmetry of the MnO_6 octahedron structure unit in $LiMnVO_4$ [12–15]. At the same time, there are visible electronic densities on the O sites in energy range III, which are consistent with the PDOS plots in figure 5(a).

The experimental insulating behavior of $LiMnVO_4$ has been reproduced successfully by the present first-principles DFT electronic structure calculations. From the band structure plots (figures 3(a) and 4) and corresponding spin projected PDOS (figures 3(c) and 5(b)) for these ordered spin states, it is evident that the intra-atomic exchange splitting of the Mn 3d spin-up and spin-down states results in an insulating gap.

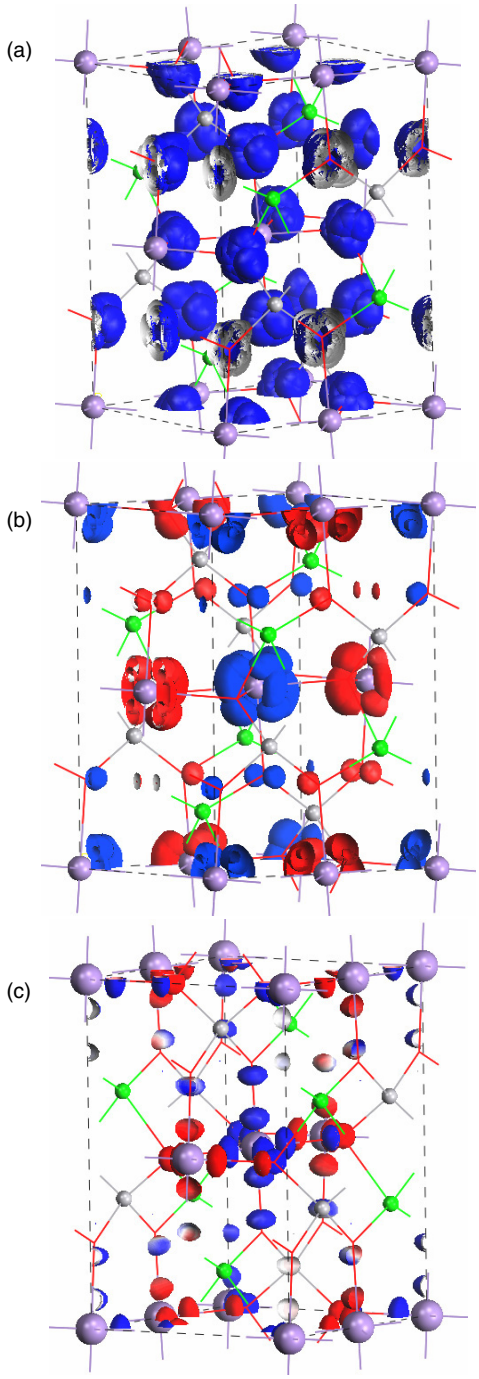

Figure 6. Isosurfaces of the electronic density for the AFM_3 state of $LiMnVO_4$ in three energy ranges. The top (a) O 2p, middle (b) Mn-t_{2g} and bottom (c) Mn-e_g correspond to the energy ranges I (-6.1 to -2.2 eV), II (-1.7 to -1.2 eV) and III (-0.4 to 0 eV). Spin-up/down electrons are paired entirely in O ions; electron density plots are just displayed for spin-up electronic states in (a).

Besides, the splitting of the Mn 3d valence bands into separated e_g bands and t_{2g} bands by the octahedral crystal field has been reproduced successfully by the present DFT calculations, which is consistent with the local crystal symmetry of the MnO_6 octahedron [12–15]. In addition, the high-spin $3d^5$ configuration of the Mn^{2+} ion and the tetrahedrally coordinated V^{5+} ion have also been simulated successfully.

3.2. Exchange interactions

The spin exchange parameters can be obtained by fitting experimental magnetic susceptibility, neutron inelastic scattering or Raman scattering measurements [33]. Besides, several theoretical methods have been used widely to evaluate exchange coupling constants in magnetic solids, such as the molecular orbital (MO) method, the valence bond (VB) method and the broken symmetry (BS) method [34]. In particular, through first-principles spin-polarized electronic structure calculations, techniques based on DFT combined with the BS approach were developed rapidly and applied extensively to quantitatively evaluate the spin exchange interactions in magnetic solids, such as in the three-dimensional AFM ordered compound $CuMnVO_4$ [32], the Cr_8 AFM molecular ring [35] and Li_2CuO_2 containing one-dimensional CuO_2 ribbon chains [36] as well as the layered compound $SrFeO_2$ [37].

Based on electronic band structure calculations for various spin-ordered magnetic insulating states of a magnetic solid, we can fit the spin exchange constants by mapping the energies onto the Heisenberg or Ising Hamiltonian with the BS approach [32, 35–37]. The spin exchange interactions in $LiMnVO_4$ can be described in terms of the exchange coupling parameters J_{intra} and J_{inter}, which are the intra-chain and inter-chain NN spin exchange parameters for the edge-sharing MnO_4 chains, respectively. The spin Hamiltonian for $LiMnVO_4$ is described by the Heisenberg model, which is written as

$$H = -J_{\text{intra}} \sum_{\langle i,j \rangle} S_i \cdot S_j - J_{\text{inter}} \sum_{\langle i,j \rangle} S_i \cdot S_j \tag{1}$$

where the S_i represents a spin operator at site i of the compound. The negative and the positive value of J in equation (1) indicate AFM or FM interactions, respectively.

In $LiMnVO_4$, the Mn^{2+} ions are in a high-spin state with $3d^5$ configurations, so the unpaired electrons are 5 per formula unit (f.u.). According to Noodleman's BS methods [24–26], the spin exchange interaction energies (per f.u.) of the FM, AFM_1, AFM_2 and AFM_3 states are written as

$$\begin{aligned} E_{\text{FM}} &= \tfrac{25}{4}(-J_{\text{intra}} - 2J_{\text{inter}}) \\ E_{\text{AFM1}} &= \tfrac{25}{4}(-J_{\text{intra}} + 2J_{\text{inter}}) \\ E_{\text{AFM2}} &= \tfrac{25}{4}(J_{\text{intra}} - 2J_{\text{inter}}) \\ E_{\text{AFM3}} &= \tfrac{25}{4}(J_{\text{intra}} + 2J_{\text{inter}}). \end{aligned} \tag{2}$$

Therefore, the spin exchange parameters, J_{intra} and J_{inter}, are mapped from the energy difference ΔE between these magnetic ordered states as

$$\begin{aligned} J_{\text{intra}} &= \tfrac{2}{25}(E_{\text{AFM2}} - E_{\text{FM}}) \\ \text{or} \qquad J_{\text{intra}} &= \frac{2}{25}(E_{\text{AFM3}} - E_{\text{AFM1}}) \\ J_{\text{inter}} &= \tfrac{1}{25}(E_{\text{AFM3}} - E_{\text{AFM2}}) \\ \text{or} \qquad J_{\text{inter}} &= \tfrac{1}{25}(E_{\text{AFM1}} - E_{\text{FM}}). \end{aligned} \tag{3}$$

Using the calculated energy values as listed in table 2, we can obtain the energy difference:

$$E_{\mathrm{AFM2}} - E_{\mathrm{FM}} = -26.5\ \mathrm{meV}$$

$$E_{\mathrm{AFM3}} - E_{\mathrm{AFM1}} = -25.7\ \mathrm{meV}$$

$$E_{\mathrm{AFM3}} - E_{\mathrm{AFM2}} = -6.8\ \mathrm{meV}$$

$$E_{\mathrm{AFM1}} - E_{\mathrm{FM}} = -7.6\ \mathrm{meV}.$$

We obtain the exchange parameters $J_{\mathrm{intra}}/k_{\mathrm{B}} = -24.2$ K and $J_{\mathrm{inter}}/k_{\mathrm{B}} = -3.3$ K. (Here the negative values denote AFM coupling interactions. We adopt the average value obtained from equation (3).) The calculated ratio of $J_{\mathrm{intra}}/J_{\mathrm{inter}}$ is approximately 8, which implies that the inter-chain AFM interactions are much weaker than intra-chain AFM interactions. The calculated $J_{\mathrm{intra}}/J_{\mathrm{inter}}$ ratio in $CuMnVO_4$ is approximately 10, which is greater than the value deduced from the susceptibility fitting [32]. Due to the lack of sufficient experimental information, we cannot perform a comprehensive comparison of our theoretical calculated exchange coupling constants with experimentally observed values available so far. However, as revealed in table 2, the calculated energy differences between the FM and AFM_1 states, as well as the AFM_2 and AFM_3 states, are very small, which reflects the weak inter-chain interactions in $LiMnVO_4$. The present quantitative calculated results indicate clearly that both the inter-chain and intra-chain spin exchange interactions are AFM and that the inter-chain magnetic coupling is negligible relative to the intra-chain coupling. Therefore, the magnetic insulating compound $LiMnVO_4$ can be described as a weakly coupled spin $\frac{5}{2}$ chain system.

$LiMnVO_4$ contains chains of edge-sharing MnO_6 octahedra running along the c axis. The Mn–O–Mn bond angles are fairly close to 90° [12, 14, 15]. The question arises of why the intra-chain Mn–Mn superexchange interaction is AFM, while the well known GKA rules [19] predict an FM superexchange interaction for the nearly 90° Mn–O–Mn configuration. As shown in figure 1, the MnO_6 octahedra are connected by pairs of edge-sharing LiO_4 and VO_4 tetrahedra. The presence of LiO_4 and VO_4 side groups coupled to ligands may contribute significantly to the AFM superexchange interaction for the nearly 90° Mn–O–Mn configuration in chains of edge-sharing MnO_6 octahedra [23]. In contrast to the usual case, this factor can significantly modify the superexchange interaction and even change the sign of the superexchange interaction. In certain cases, this factor can cause an apparent violation of the GKA rules and make the 90° superexchange of half-filled shells antiferromagnetic. The side group effects were first taken into account in analysis of the magnetic properties of the spin–Peierls system $CuGeO_3$ by Geertsma and Khomskii [23]. This factor was also suggested to play an important role in the mechanism of the superexchange interaction for the edge-sharing octahedron (or square pyramid) compound $Na_2Cu_2Si_4O_{11}{\cdot}2H_2O$ ($Na_2Cu_2Si_4O_{11}$) [38].

The calculated results of the present work have suggested strong AFM intra-chain AFM interactions in the edge-sharing MnO_4 chains; whether $LiMnVO_4$ can be viewed as a 1D or quasi-1D spin chain system requires more detailed experimental investigations. Due to the ignoring of the intra-chain next-nearest-neighbor (NNN) exchange interactions in the edge-sharing MnO_4 chains in the process of the present theoretical calculations, the NN exchange coupling may compete with the NNN exchange interactions, so a spiral-magnetic ordering or other magnetic frustration may set in [20]. To prepare a high quality single crystal of $LiMnVO_4$ is all-important. Then inelastic neutron scattering and magnetic susceptibility measurements along different crystallographic axes are in dire need of being performed to determine the magnetic structure of $LiMnVO_4$. In addition, the electronic and magnetic structures of TMOs, especially the superexchange interactions, are very sensitive to their dimensionality and lattice geometry [23]. Here we propose that the presence of LiO_4 and VO_4 side groups leads to the AFM superexchange interaction for the nearly 90° Mn–O–Mn configuration in $LiMnVO_4$, therefore experimental doping or substitution may induce magnetic state transformations or other promising properties. Besides, profuse and attractive phenomena and characteristics can also be expected because of the similarity of the edge-sharing structural unit between $LiMnVO_4$ and the parent cuprate compound of high-temperature superconductors. In conclusion, $LiMnVO_4$ affords a good ground to further investigate and exploit variously intriguing phenomena and fantastic properties in the TMOs.

4. Summary and conclusions

The detailed electronic structure and magnetic properties of the spinel-related structural compound $LiMnVO_4$ have been investigated by fully self-consistent *ab initio* DFT calculations. The experimental insulating behavior has been successfully reproduced by spin-polarized GGA calculations for four possible spin-ordered states. The exchange splitting of the Mn 3d spin-up and spin-down states results in an insulating gap. The $3d^5$ configurations of the octahedrally coordinated high-spin Mn^{2+} ions and tetrahedrally coordinated V^{5+} ($3d^0$) ions have been successfully simulated. The ground state of $LiMnVO_4$ is the AFM state with both intra-chain and inter-chain magnetic moments AFM aligned.

The spin exchange parameters are deduced by mapping the energies of the four ordered spin states onto the Heisenberg Hamiltonian within Noodleman's broken symmetry method. The calculated exchange constants indicate that the intra-chain AFM interactions are much stronger than the inter-chain AFM interactions. We propose that the presence of the side groups of pairs of edge-sharing LiO_4 and VO_4 tetrahedra has caused the intra-chain AFM interactions in the edge-sharing MnO_4 chains with nearly 90° Mn–O–Mn bond angles. $LiMnVO_4$ is a weakly coupled edge-sharing MnO_4 AFM chain system.

Acknowledgments

This work was sponsored by both the Chinese National Science Foundation under grant No 50672031 and the Program for Changjiang Scholar and Innovative Research Team in University under grant No IRT0625. This work was also

partially supported by MOST of China under grant No 2007CB216406 and the Scientific and Technologic Research and Development program of Jilin Province, China, under grant No 20060511.

References

[1] Tokura Y and Nagaosa N 2000 *Science* **288** 462
[2] Croft M, Kiryukhin V, Horibe Y and Cheong S-W 2007 *New J. Phys.* **9** 86
[3] Radaelli P G 2005 *New J. Phys.* **7** 53
[4] Amatucci G and Tarascon J-M 2002 *J. Electrochem. Soc.* **149** K31
[5] Lee S T, Raveendranath K, Tomy M R, Paulraj M, Jayalekshmi S and Ravi J 2007 *Appl. Phys. Lett.* **90** 161912
[6] Lee S T, Raveendranath K, Tomy M R, Paulraj M, Jayalekshmi S, Nair K P R and Ravi J 2007 *Phys. Rev.* B **76** 115112
[7] Tomeno I, Kasuya Y and Tsunoda Y 2001 *Phys. Rev.* B **64** 094422
[8] Kondo S, Johnston D C, Swenson C A, Borsa F, Mahajan A V, Miller L L, Gu T, Goldman A I, Maple M B, Gajewski D A, Freeman E J, Dilley N R, Dickey R P, Merrin J, Kojima K, Luke G M, Uemura Y J, Chmaissem O and Jorgensen J D 1997 *Phys. Rev. Lett.* **78** 3729
[9] Shimoyamada A, Tsuda S, Ishizaka K, Kiss T, Shimojima T, Togashi T, Watanabe S, Zhang C Q, Chen C T, Matsushita Y, Ueda H, Ueda Y and Shin S 2006 *Phys. Rev. Lett.* **96** 026403
[10] Das S, Zong X, Niazi A, Ellern A, Yan J Q and Johnston D C 2007 *Phys. Rev.* B **76** 054418
[11] Arita R, Held K, Lukoyanov A V and Anisimov V I 2007 *Phys. Rev. Lett.* **98** 166402
[12] Sato M and Kano S 1994 *Chem. Lett.* **23** 427
[13] Sato M, Kano S, Tamaki S, Misawa M, Shirakawa Y and Ohashi M 1996 *J. Mater. Chem.* **6** 1191
[14] Padhi A K, Archibald W B, Nanjundaswamy K S and Goodenough J B 1997 *J. Solid State Chem.* **128** 267
[15] Sugahara M, Yoshiasa A, Yamanaka T and Takei H 2003 *Acta Crystallogr.* E **59** i161
[16] Suzuki S, Tomita M, Okada S and Arai H 1997 *J. Phys. Chem. Solids* **58** 799
[17] Rissouli K, Benkhouja K, Touaiher M and Julien C M 2003 *Lithium and Lithium-Ion Batteries* vol 28 (New Jersey: Electrochemical Society) p 315
[18] Schwingenschlögl U and Schuster C 2007 *Phys. Rev. Lett.* **99** 237206
[19] Goodenough J B 1955 *Phys. Rev.* **100** 564
Kanamori J 1959 *J. Phys. Chem. Solids* **10** 87
Anderson P W 1963 *Solid State Phys.* **14** 99
[20] Büttgen N, Krug von Nidda H-A, Svistov L E, Prozorova L A, Prokofiev A and Aßmus W 2007 *Phys. Rev.* B **76** 014440
[21] Park S, Choi Y J, Zhang C L and Cheong S-W 2007 *Phys. Rev. Lett.* **98** 057601
[22] Mizuno Y, Tohyama T, Maekawa S, Osafune T, Motoyama N, Eisaki H and Uchida S 1998 *Phys. Rev.* B **57** 5326
[23] Geertsma W and Khomskii D 1996 *Phys. Rev.* B **54** 3011
[24] Noodleman L 1981 *J. Chem. Phys.* **74** 5737
[25] Noodleman L and Davidson E R 1986 *Chem. Phys.* **109** 131
[26] Noodleman L and Case D A 1992 *Adv. Inorg. Chem.* **38** 423
[27] Segall M D, Lindan P J D, Probert M J, Pickard C J, Hasnip P J, Clark S J and Payne M C 2002 *J. Phys.: Condens. Matter* **14** 2717
[28] Perdew J P, Burke K and Ernzerhof M 1996 *Phys. Rev. Lett.* **77** 3865
[29] Perdew J P, Chevary J A, Vosko S H, Jackson K A, Pederson M R, Singh D J and Fiolhais C 1992 *Phys. Rev.* B **46** 6671
[30] Vanderbilt D 1990 *Phys. Rev.* B **41** 7892
[31] Pfrommer B G, Côté M, Louie S G and Cohen M L 1997 *J. Comput. Phys.* **131** 133
[32] Yahia H B, Gaudin E, Darriet J, Banks M, Kremer R K, Villesuzanne A and Whangbo M-H 2005 *Inorg. Chem.* **44** 3087
[33] Dai D and Whangbo M-H 2001 *J. Chem. Phys.* **114** 2887
[34] Mouesca J-M 2000 *J. Chem. Phys.* **113** 10505
[35] Bellini V, Olivieri A and Manghi F 2006 *Phys. Rev.* B **73** 184431
[36] Xiang H J, Lee C and Whangbo M-H 2007 *Phys. Rev.* B **76** 220411
[37] Xiang H J, Wei S-H and Whangbo M-H 2008 *Phys. Rev. Lett.* **100** 167207
[38] dos Santos A M, Amaral V S, Brandão P, Almeida Paz F A, Rocha J, Ferreira L P, Godinho M, Volkova O and Vasiliev A 2005 *Phys. Rev.* B **72** 092403